American Mineralogist, Volume 79, pages 1176–1184, 1994

Structural variations induced by heat treatment in allanite and REE-bearing piemontite

Paola Bonazzi, Silvio Menchetti
Dipartimento di Scienze della Terra, Università di Firenze, via La Pira 4, I-50121, Florence, Italy

Abstract

In REE-bearing minerals of the epidote group, the presence of trivalent rare earth elements substituting for Ca requires the entry of divalent cations (Fe^{2+}, Mn^{2+}, Mg) in the octahedral sites. Upon heating allanite and REE-bearing piemontite in air, Fe^{2+} and Mn^{2+} oxidize; however, the charge balance is maintained by a corresponding H loss. The present work deals with the structural adjustments involved in this process. To this purpose, two single crystals (allanite and REE-bearing piemontite) were selected for heat treatments and structural study. Crystals were annealed in air for 48 h at several temperatures between 380 and 900 °C. After each heat treatment, unit-cell parameters were determined. Structure refinements were performed whenever significant variations in the lattice parameters took place, and structural changes occurring with the increase of the heating temperature were examined. Oxidation mainly resulted in a shortening of the mean M3-O octahedral distances and, to a lesser extent, of the mean M1-O distances; dehydrogenation was made evident by a dramatic lengthening of the donor to acceptor distance, as well as by the compensational shortening of the bond distances involving the O10 in OH. Heat treatments also induced a minor migration of octahedral cations, as inferred from changes in the number of electrons deriving from the site-occupancy refinement. The oxidation-dehydrogenation process caused variations in the unit-cell parameters. In particular, a shortening of *b* (which is parallel to the octahedral chains) was observed in the treated allanite crystal. In the sample of REE-bearing piemontite, the increase of Mn^{3+}, due to the oxidation of Mn^{2+}, caused a stronger Jahn-Teller effect on the M3 octahedron, resulting in a shortening of the octahedron along the **a** axis; therefore, the *a* parameter decreased more than *b* for increasing annealing temperature. In both allanite and REE-piemontite, the relaxing of the H bond, directed along the **c** axis, resulted in a lengthening of the *c* parameter. As the oxyallanite component increased, a corresponding increase in the value of β was observed.

Introduction

The general formula for the epidote minerals can be written $A_2M_3(SiO_4)(Si_2O_7)(O,F)(OH)$, where A = Ca, Sr, Pb^{2+}, Mn^{2+}, REE^{3+}, Th, and U and where M = Al, Fe^{3+}, Mn^{3+}, Fe^{2+}, Mn^{2+}, and Mg.

In the REE-bearing epidote minerals, the substitution of trivalent rare earth elements for Ca in the A2 site requires the presence of divalent cations in the octahedral positions, in which the REE-free members are occupied exclusively by trivalent cations. The coupled substitution $Ca + (Fe^{3+},Mn^{3+},Al) \rightleftharpoons REE^{3+} + (Fe^{2+},Mn^{2+},Mg)$ can describe the complex isomorphous relationships occurring among the epidote-group minerals containing rare earth elements. The dominant octahedral divalent cation is Fe^{2+} in allanite (Ueda, 1955; Rumanova and Nikolaeva, 1960; Khvostova, 1963; Dollase, 1971) and Mg in both dissakisite (Grew et al., 1991; Rouse and Peacor, 1993) and dollaseite (Peacor and Dunn, 1988); minerals of this group with Mn^{2+} prevailing in the M3 site have also been found (Sokolova et al., 1991; Bonazzi et al., 1993). An additional mechanism that could balance the entry of REE^{3+} is the heterovalent substitution $OH^- \rightleftharpoons O^{2-}$, as recently suggested by Rouse and Peacor (1993) for the structure of dissakisite-(Ce). The hypothesis that the composition of allanite may extend toward the oxyallanite component was considered by Grew et al. (1991). These authors, taking into account numerous chemical data from the literature, observed that variation in Ca does not correlate with variation in M^{3+} (i.e., Al + Fe^{3+}); this was tentatively attributed to an additional substitutional mechanism such as $(Fe^{2+},Mg) + OH^- \rightleftharpoons (Fe^{3+},Al) + O^{2-}$, which leads to an ideal oxyallanite end-member $CaREE(Al,Fe^{3+})_3Si_3O_{13}$. However, the hypothesis that allanite is sometimes lacking in H is not easy to verify due to the scarcity of direct terminations of the H_2O content and possible errors in the analytical data.

In the case of nonmetamict samples, geometrical and structural parameters could tentatively be used to evaluate the H content in the structure, but single-crystal data

0003–004X/94/1112–1176$02.00

relating to oxidized allanite have not been published to date. This is surprising, given that allanite with a high content of the oxyallanite component is easy to obtain by heat treatment. On heating allanite in air, Fe^{2+} oxidizes and the charge balance is maintained by a corresponding loss of H. The following scheme may describe the reaction in terms of a coupled substitution: $Fe^{2+} + OH^- \rightleftharpoons Fe^{3+} + O^{2-}$. The allanite → oxyallanite transformation was previously studied by Dollase (1973) by means of Mössbauer spectroscopy on a sample from the Paicoma Canyon. In accordance with the findings of this author, the reaction, which appears to be more temperature-dependent than time-dependent, starts above 400 °C and is essentially completed at about 700 °C. The Fe^{3+}-Fe^{2+} ratio can be varied continuously by increasing the temperature and reversed to the original value by treatment under an H_2 atmosphere. On the basis of powder spectra of natural and heated samples, Kumskova and Khvostova (1964) showed that by heating allanite, slight changes are induced in its diffraction pattern, which becomes more like that of epidote. Analogous treatments on epidote do not, however, produce any change in the *d* values. Janeczek and Eby (1993) conducted annealing experiments on allanite with different degrees of metamictization under an Ar atmosphere. They studied changes in unit-cell parameters by means of powder X-ray diffraction; however, the variations were due mainly to the progressive restoring of the crystallinity that occurs with annealing.

The present work deals with the structural adjustments involved in the oxidation-dehydrogenation process of allanite. In addition, the different effects produced by the oxidation of Fe and Mn, respectively, are discussed: to this purpose the heating experiments were performed on both allanite and REE-bearing piemontite.

Samples

Crystals selected for heat treatments and structural study were allanite (sample BG2) and REE-bearing piemontite (sample BR16a), respectively; the first comes from a granitic rock of the Rhodope Massif, Bulgaria (sample no. 1105/RI, Mineralogical Museum of the University of Florence), the second from Mount Brugiana, Alpi Apuane, Italy (Bonazzi et al., 1992).

To verify that no significant variations in lattice parameters are induced by heating when oxidizable divalent cations are not present, two REE-free crystals, HMC1 and SM19, were also studied. Sample HMC1 is an epidote crystal from an exoskarn associated with the Gangwei monzonitic granite at Maanshan, Guangdong Province, China (IGAS CSMPG, 1987). Sample SM19 is a Sr-rich piemontite crystal from the type-locality Saint Marcel, Valle d'Aosta, Italy (Mottana and Griffin, 1982).

Experimental methods

Structure refinements of samples BG2 and BR16a were performed before the heat treatment; subsequently, the same crystals, together with samples HMC1 and SM19, were prepared to carry out chemical analyses. Chemical data and experimental conditions used for electron microprobe analyses are given in Table 1. Crystals were subsequently removed from the resin, and structure refinements (BG2, BR16a) were repeated, thus making it possible to compare the structural data obtained from the same portion of the crystal before and after the heating experiments. All the crystals were annealed in air for 48 h at selected temperatures ranging from 380 °C to the temperature at which the structure breaks down (in steps of 25–50 °C). After each treatment, the crystals were cooled to room temperature, and lattice parameters were determined (Table 2) by means of least-squares refinements using 25 high-θ reflections measured with a CAD4 single-crystal diffractometer. The same crystals were used for the next annealing experiment at a higher temperature. Whenever significant variations in the unit-cell dimensions took place, intensity data were collected and corrected for Lorentz-polarization and absorption effects (North et al., 1968). No changes in symmetry or systematic absences (consistent with the $P2_1/m$ space group) were observed until the breakdown of the structure. Structure refinements were performed using the program SHELX (Sheldrick, 1976). Scattering factors (ionized atoms) and

Table 1. Chemical composition (wt%) and atomic proportions of the single crystal studied

	BR16a	BG2	HMC1	SM19
SiO_2	34.23	31.85	37.19	35.48
Al_2O_3	18.24	18.36	23.14	18.85
Mn_2O_3*	12.99	0.22	0.57	15.82
Fe_2O_3*	5.61	13.82	14.35	1.96
MgO	0.48	1.32	—	—
TiO_2	—	0.61	—	—
CaO	16.96	11.45	22.90	20.56
SrO	0.29	—	—	3.94
Y_2O_3	—	0.08	—	—
La_2O_3	3.13	6.07	—	—
Ce_2O_3	1.32	10.54	—	—
Pr_2O_3	0.53	0.89	—	—
Nd_2O_3	1.60	2.84	—	—
Sm_2O_3	0.10	0.20	—	—
Gd_2O_3	—	0.10	—	—
ThO_2	—	0.91	—	—
Total	95.48	99.26	98.15	96.61
Si	2.998	2.944	2.968	2.971
Al	1.883	2.000	2.177	1.861
Mn	0.866	0.016	0.035	1.008
Fe	0.370	0.962	0.862	0.124
Mg	0.062	0.182	—	—
Ti	—	0.042	—	—
Ca	1.592	1.134	1.958	1.845
Sr	0.015	—	—	0.191
Y	—	0.004	—	—
La	0.101	0.207	—	—
Ce	0.042	0.357	—	—
Pr	0.018	0.030	—	—
Nd	0.050	0.094	—	—
Sm	0.003	0.006	—	—
Gd	—	0.003	—	—
Th	—	0.019	—	—
O*	12.665	12.845	12.505	12.468

Note: total cations = 8.0. Equipment: ARL SEMQ. Lines used: $K\alpha$ (Mg,Al,Si,Ca,Ti,Mn,Fe); $L\alpha$ (Sr,La,Ce); $L\beta$ (Nd,Pr,Sm); $M\alpha$ (Th).

* Mn_2O_3 and Fe_2O_3 as Mn_{tot} and Fe_{tot}, respectively; for BR16a and BG2, the effective number of O atoms, >12.5, is consistent with the presence of Mn and Fe in the lower valence state. H_2O was not determined.

Table 2. Unit-cell parameters determined after each heat treatment

T (°C)	BG2 a (Å)	b (Å)	c (Å)	β (°)	V (Å³)	BR16a a (Å)	b (Å)	c (Å)	β (°)	V (Å³)
RT	8.902(1)	5.713(1)	10.127(1)	114.86(1)	467.3(1)	8.878(1)	5.681(1)	10.146(1)	115.04(1)	463.6(1)
380	8.897(1)	5.709(1)	10.114(1)	114.82(1)	466.3(1)	8.876(1)	5.680(1)	10.147(1)	115.02(1)	463.6(1)
450	8.895(1)	5.709(1)	10.108(1)	114.82(1)	465.9(1)	8.876(1)	5.681(1)	10.143(1)	115.01(1)	463.5(1)
500	8.891(1)	5.706(1)	10.107(1)	114.82(1)	465.3(1)	8.875(1)	5.680(1)	10.146(1)	115.01(1)	463.5(1)
550	8.894(1)	5.703(1)	10.109(1)	114.86(1)	465.2(1)	8.876(1)	5.679(1)	10.150(1)	115.04(1)	463.5(1)
600	8.887(1)	5.701(1)	10.109(1)	114.84(1)	464.8(1)	8.875(1)	5.679(1)	10.156(1)	115.09(1)	463.6(1)
650	8.885(5)	5.682(2)	10.148(6)	115.06(5)	464.1(5)	8.870(1)	5.677(1)	10.171(1)	115.15(1)	463.6(1)
675	8.869(2)	5.657(1)	10.302(2)	115.59(2)	466.2(2)	8.868(1)	5.676(1)	10.181(1)	115.20(1)	463.7(1)
700	8.873(1)	5.649(1)	10.331(1)	115.64(2)	466.8(2)	8.867(1)	5.676(1)	10.190(1)	115.24(1)	463.9(1)
725	8.871(1)	5.647(1)	10.352(1)	115.67(1)	467.4(1)	8.862(1)	5.675(1)	10.199(1)	115.28(1)	463.8(1)
750	8.870(1)	5.648(1)	10.357(1)	115.72(1)	467.4(1)	8.859(1)	5.675(1)	10.207(1)	115.31(1)	463.9(1)
775	8.867(2)	5.648(1)	10.363(1)	115.73(1)	467.5(1)					
800	8.870(1)	5.646(1)	10.365(1)	115.71(1)	467.7(1)	8.856(1)	5.674(1)	10.228(1)	115.44(1)	464.1(1)
825	8.871(1)	5.646(1)	10.360(1)	115.74(1)	467.4(1)					
850	8.872(1)	5.646(1)	10.367(1)	115.76(1)	467.7(1)	8.854(1)	5.671(1)	10.244(1)	115.53(1)	464.1(1)
880	8.874(2)	5.646(1)	10.370(2)	115.78(1)	467.9(2)	8.853(1)	5.670(1)	10.244(1)	115.52(1)	464.0(1)
905	8.868(2)	5.646(1)	10.369(2)	115.75(2)	467.6(2)	8.851(1)	5.672(1)	10.241(1)	115.54(1)	463.9(1)
930	8.848(5)	5.628(6)	10.396(9)	115.97(7)	465.4(7)					
T (°C)	HMC1 a (Å)	b (Å)	c (Å)	β (°)	V (Å³)	SM19 a (Å)	b (Å)	c (Å)	β (°)	V (Å³)
RT	8.900(1)	5.643(1)	10.168(1)	115.40(1)	461.3(1)	8.867(2)	5.681(1)	10.186(1)	115.26(1)	464.0(1)
500	8.899(1)	5.642(1)	10.168(1)	115.38(1)	461.2(1)	8.867(1)	5.681(1)	10.186(1)	115.27(1)	464.0(1)
600	8.898(1)	5.643(1)	10.168(1)	115.38(1)	461.3(1)	8.863(1)	5.680(1)	10.184(2)	115.25(1)	463.7(1)
700	8.900(1)	5.642(1)	10.168(1)	115.40(1)	461.3(1)	8.864(1)	5.680(1)	10.186(2)	115.25(1)	463.8(1)
800	8.901(1)	5.644(1)	10.173(1)	115.41(1)	461.6(1)	8.867(2)	5.680(1)	10.190(1)	115.27(1)	464.1(1)
850	8.896(1)	5.644(1)	10.177(1)	115.43(1)	461.5(1)	8.866(2)	5.677(1)	10.200(1)	115.31(1)	464.1(1)

the correction factors for anomalous dispersion were taken from the *International Tables for X-ray Crystallography* (Ibers and Hamilton, 1974). Other details of the experimental work (related to the intensity data collection) are given in Table 3. No structure refinements were performed on HMC1 and SM19, since no significant variations in the unit-cell parameters were induced by heating.

Table 3. Intensity data collection and structure refinement information

	BG2		
θ range		MoKα	2–35°
Scan mode			ω
Scan width			3.00°
Scan speed			4.1°/min
T (°C)	R_{symm}	R_{obs}	N_{obs}
RT	1.49	1.75	2083
380	1.69	1.76	2094
550	1.95	2.21	2124
650	1.45	6.34	2114
725	1.44	1.59	1705
800	1.46	1.70	1732
	BR16a		
θ range		MoKα	2–35°
Scan mode			ω
Scan width			2.60°
Scan speed			3.3°/min
T (°C)	R_{symm}	R_{obs}	N_{obs}
RT	1.52	2.07	1600
550	1.48	1.90	1634
650	1.45	1.85	1608
725	1.43	1.70	1585
800	1.40	1.77	1614
880	1.40	1.74	1608

Note: $R_{symm} = (\Sigma \{N \Sigma [w(\bar{F}_o - F_o)^2]\}/\Sigma [(N-1) \Sigma (wF_o^2)])^{1/2}$. $R_{obs} = \Sigma (w^{1/2}|F_o - F_c|)/\Sigma (w^{1/2}F_o)$. N_{obs} = no. of reflections with $F_o > 8\sigma(F_o)$.

To give an estimate of the original Fe^{2+}-Fe^{3+} ratio in the untreated sample, a wet-chemical analysis was performed on the allanite from the Rhodope Massif according to the method of Shapiro and Brannock (1962). The results are as follows: Fe_2O_3 13.65 wt%, FeO 9.05 wt%. The amount of FeO determined after a heat treatment at 725 °C was 0.80 wt%. An analogous determination on the REE-bearing piemontite from Mount Brugiana was not performed, since it was judged meaningless because of the very wide range of values shown by the REE^{3+} content (previous microprobe analyses).

Discussion

Bond distances and mean electron numbers derived from the structure refinements are given in Tables 4 and 5 for BG2 and BR16a, respectively; lists of observed and calculated structure factors are available from the authors. The structural rearrangement observed with the increase of the heating temperature is mainly the result of the local charge imbalance associated with the ongoing oxidation and dehydrogenation processes. The oxidizable cations (Fe^{2+} in allanite, Mn^{2+} in piemontite) are located in the M3 site; however, Dollase (1971, 1973) and Bonazzi and Menchetti (1994) hypothesized that small amounts of divalent cations can also enter the M1 site. It should be noted (Fig. 1) that neither M3 nor M1 are bonded to the O atom in OH (O10), so that the undersaturation on O10, which accompanies the H loss, cannot be offset locally by Fe oxidation. The amphibole → oxyamphibole

TABLE 4. Structural parameters for crystal BG2

	RT	380 °C	550 °C	650 °C	725 °C	800 °C
A1-O3 (× 2)	2.333(1)	2.330(2)	2.329(2)	2.316(5)	2.316(2)	2.320(2)
A1-O7	2.338(2)	2.332(3)	2.331(3)	2.315(8)	2.325(3)	2.327(3)
A1-O1 (× 2)	2.382(1)	2.382(2)	2.382(2)	2.395(5)	2.432(2)	2.430(2)
A1-O5	2.586(2)	2.585(2)	2.585(3)	2.517(6)	2.508(2)	2.507(2)
A1-O6	2.897(2)	2.894(2)	2.889(2)	2.903(5)	2.946(2)	2.953(2)
⟨A1-O⟩	2.465	2.462	2.461	2.451	2.468	2.470
No. *e* (A1)	20.5	20.7	20.7	20.9	20.0	19.7
A2-O7	2.318(2)	2.317(2)	2.314(3)	2.312(7)	2.300(2)	2.295(2)
A2-O2 (× 2)	2.484(1)	2.481(2)	2.482(2)	2.498(5)	2.587(1)	2.593(2)
A2-O10	2.608(2)	2.613(2)	2.607(2)	2.500(5)	2.355(2)	2.359(2)
A2-O2′ (× 2)	2.659(2)	2.658(2)	2.663(2)	2.723(5)	2.803(2)	2.797(2)
A2-O3 (× 2)	2.774(1)	2.771(2)	2.759(2)	2.711(5)	2.641(2)	2.637(2)
⟨A2-O⟩	2.595	2.594	2.591	2.585	2.590	2.589
No. *e* (A2)	48.2	48.1	47.7	47.8	48.1	48.6
M1-O4 (× 2)	1.854(1)	1.855(1)	1.851(1)	1.840(4)	1.831(1)	1.830(1)
M1-O1 (× 2)	1.966(1)	1.966(2)	1.964(2)	1.961(5)	1.956(2)	1.955(2)
M1-O5 (× 2)	1.992(1)	1.991(1)	1.987(1)	1.997(5)	2.000(2)	2.000(2)
⟨M1-O⟩	1.937	1.937	1.934	1.933	1.929	1.929
λ	1.0065	1.0063	1.0065	1.0071	1.0075	1.0076
σ^2	16.05	15.52	16.19	16.49	16.69	17.00
No. *e* (M1)	14.7	14.7	14.8	15.2	15.4	15.1
M2-O3 (× 2)	1.866(1)	1.865(2)	1.865(2)	1.876(4)	1.896(2)	1.904(2)
M2-O10 (× 2)	1.891(2)	1.893(2)	1.890(2)	1.877(5)	1.844(2)	1.844(2)
M2-O6 (× 2)	1.920(2)	1.918(2)	1.919(2)	1.922(5)	1.962(2)	1.966(2)
⟨M2-O⟩	1.892	1.892	1.891	1.892	1.900	1.904
λ	1.0060	1.0059	1.0059	1.0062	1.0060	1.0059
σ^2	20.54	20.16	19.92	20.98	16.90	16.33
No. *e* (M2)	13.0	13.0	13.1	13.3	13.8	14.8
M3-O8	1.936(2)	1.937(2)	1.934(2)	1.919(6)	1.893(3)	1.890(3)
M3-O4	1.976(2)	1.977(2)	1.973(3)	1.948(5)	1.907(2)	1.898(2)
M3-O2 (× 2)	2.148(1)	2.150(2)	2.138(2)	2.096(5)	2.016(2)	2.011(2)
M3-O1 (× 2)	2.275(1)	2.272(2)	2.266(2)	2.263(5)	2.272(2)	2.277(2)
⟨M3-O⟩	2.126	2.126	2.119	2.097	2.063	2.061
λ	1.0401	1.0404	1.0394	1.0362	1.0333	1.0338
σ^2	116.94	118.37	115.34	102.39	85.76	85.38
No. *e* (M3)	22.6	22.5	22.4	22.3	22.5	22.1
Si1-O7	1.588(2)	1.590(2)	1.585(2)	1.581(5)	1.578(2)	1.580(2)
Si1-O1 (× 2)	1.638(1)	1.636(2)	1.639(2)	1.640(5)	1.644(2)	1.641(2)
Si1-O9	1.641(3)	1.642(3)	1.642(4)	1.621(9)	1.632(3)	1.632(4)
⟨Si1-O⟩	1.626	1.626	1.626	1.620	1.625	1.623
λ	1.0028	1.0028	1.0029	1.0031	1.0028	1.0028
σ^2	9.71	9.88	10.00	9.58	8.37	8.85
Si2-O8	1.593(2)	1.596(3)	1.594(3)	1.611(9)	1.606(3)	1.601(3)
Si2-O3 (× 2)	1.627(1)	1.629(1)	1.628(2)	1.618(4)	1.611(2)	1.612(2)
Si2-O9	1.636(2)	1.635(2)	1.631(3)	1.628(8)	1.628(2)	1.627(3)
⟨Si2-O⟩	1.621	1.622	1.620	1.619	1.614	1.613
λ	1.0008	1.0009	1.0009	1.0011	1.0005	1.0005
σ^2	2.96	3.23	3.35	4.32	1.86	1.92
Si3-O2 (× 2)	1.626(2)	1.623(2)	1.623(2)	1.625(5)	1.639(2)	1.641(2)
Si3-O6	1.647(3)	1.647(3)	1.645(4)	1.644(9)	1.628(3)	1.629(3)
Si3-O5	1.662(2)	1.661(2)	1.661(2)	1.664(6)	1.664(2)	1.662(2)
⟨Si3-O⟩	1.640	1.638	1.638	1.640	1.642	1.644
λ	1.0068	1.0070	1.0069	1.0071	1.0036	1.0034
σ^2	26.98	27.67	27.59	28.17	13.97	13.39
O10-O4	2.941(3)	2.925(3)	2.926(4)	3.000(9)	3.166(3)	3.174(3)

Note: distances are reported in ångströms; no. *e* = mean number of electrons derived from site occupancy refinement; the mean quadratic elongation (λ) and the angle variance (σ^2) were computed according to Robinson et al. (1971).

transformation, for example, is a different case: underbonding to the O3 in OH is in part directly compensated by the increase of the positive charge ($Fe^{2+} \rightarrow Fe^{3+}$) on M1 and M3, both linked to O3 (Ungaretti, 1980; Phillips et al., 1988, 1989). The variations of the bond distances and of the unit-cell parameters in both allanite and REE-bearing piemontite, which reflect the oxidation and the dehydrogenation, are discussed in the following sections.

Effects of oxidation

For the two crystals examined, oxidation of the divalent cations is made evident by a significant shortening of the mean ⟨M3-O⟩ distance (Fig. 2); the total difference between the ⟨M3-O⟩ values before and after the heat treatments is 0.065 and 0.021 Å for crystals BG2 and BR16a, respectively. Among the M3-O distances, the one most sensitive to the increase of trivalent cations appears to be M3-O2. In untreated allanite, the greater the amount of Fe^{2+} in M3, the closer the O2 atom is to the A2 cation. With increasing annealing temperature, the O2 atom moves from A2 toward M3. With the ongoing oxidation process, a moderate shortening of the ⟨M1-O⟩ distance is also observed (Tables 4 and 5); this means that divalent cations are present also at M1, thus removing the uncer-

Table 5. Structural parameters for crystal BR16a

	RT	550 °C	650 °C	725 °C	800 °C	880 °C
A1-O3 (× 2)	2.302(2)	2.303(2)	2.303(2)	2.304(2)	2.304(2)	2.304(2)
A1-O7	2.291(3)	2.292(3)	2.293(3)	2.291(3)	2.287(2)	2.291(2)
A1-O1 (× 2)	2.415(2)	2.417(2)	2.422(2)	2.429(2)	2.430(2)	2.427(2)
A1-O5	2.556(3)	2.558(2)	2.548(2)	2.541(3)	2.542(2)	2.540(2)
A1-O6	2.921(2)	2.924(2)	2.923(2)	2.936(2)	2.936(2)	2.942(2)
⟨A1-O⟩	2.457	2.459	2.459	2.462	2.462	2.462
No. *e* (A1)	20.8	20.8	20.8	20.7	20.6	20.7
A2-O7	2.281(3)	2.279(2)	2.272(2)	2.268(2)	2.270(2)	2.271(2)
A2-O2 (× 2)	2.516(2)	2.516(2)	2.525(2)	2.534(2)	2.547(1)	2.550(1)
A2-O10	2.559(3)	2.553(2)	2.522(2)	2.483(2)	2.453(2)	2.447(2)
A2-O2′ (× 2)	2.675(2)	2.679(2)	2.697(2)	2.717(2)	2.723(2)	2.727(2)
A2-O3 (× 2)	2.793(2)	2.784(2)	2.765(2)	2.751(2)	2.736(2)	2.729(2)
⟨A2-O⟩	2.601	2.599	2.596	2.594	2.592	2.591
No. *e* (A2)	31.2	31.2	31.1	31.3	31.2	31.2
M1-O4 (× 2)	1.860(1)	1.861(1)	1.864(1)	1.860(1)	1.857(1)	1.857(1)
M1-O1 (× 2)	1.975(2)	1.973(2)	1.972(2)	1.969(2)	1.959(2)	1.956(2)
M1-O5 (× 2)	1.995(2)	1.992(1)	1.995(1)	1.996(1)	1.995(1)	1.995(1)
⟨M1-O⟩	1.943	1.942	1.944	1.942	1.937	1.936
λ	1.0059	1.0059	1.0057	1.0062	1.0065	1.0065
σ^2	14.17	14.53	14.06	15.38	16.57	16.43
No. *e* (M1)	16.8	17.0	17.3	17.5	16.8	16.6
M2-O3 (× 2)	1.859(2)	1.858(2)	1.859(2)	1.863(2)	1.874(2)	1.875(2)
M2-O10 (× 2)	1.881(2)	1.882(2)	1.878(2)	1.873(2)	1.871(2)	1.867(2)
M2-O6 (× 2)	1.922(2)	1.922(2)	1.924(2)	1.931(2)	1.944(2)	1.945(2)
⟨M2-O⟩	1.887	1.887	1.887	1.889	1.896	1.896
λ	1.0056	1.0055	1.0056	1.0056	1.0053	1.0054
σ^2	18.50	18.01	18.47	17.99	16.63	16.75
No. *e* (M2)	13.0	13.0	13.0	13.4	14.6	15.2
M3-O8	1.900(3)	1.899(3)	1.888(3)	1.878(3)	1.867(3)	1.864(3)
M3-O4	1.957(3)	1.949(2)	1.940(2)	1.924(3)	1.905(2)	1.896(2)
M3-O2 (× 2)	2.066(2)	2.065(2)	2.054(2)	2.041(2)	2.034(2)	2.025(2)
M3-O1 (× 2)	2.252(2)	2.253(2)	2.255(2)	2.259(2)	2.267(2)	2.277(2)
⟨M3-O⟩	2.082	2.081	2.074	2.067	2.062	2.061
λ	1.0332	1.0334	1.0327	1.0328	1.0338	1.0347
σ^2	93.08	92.72	88.49	85.73	85.16	85.34
No. *e* (M3)	24.2	24.1	23.8	23.7	23.1	22.8
Si1-O7	1.579(2)	1.578(2)	1.577(2)	1.576(2)	1.574(2)	1.571(2)
Si1-O1 (× 2)	1.647(2)	1.648(2)	1.648(2)	1.645(2)	1.648(2)	1.647(2)
Si1-O9	1.637(3)	1.636(3)	1.638(3)	1.636(4)	1.638(3)	1.637(3)
⟨Si1-O⟩	1.627	1.628	1.628	1.626	1.627	1.625
λ	1.0029	1.0028	1.0028	1.0027	1.0029	1.0029
σ^2	9.14	8.75	8.75	8.22	8.85	8.83
Si2-O8	1.600(3)	1.602(3)	1.601(3)	1.603(3)	1.600(3)	1.599(3)
Si2-O3 (× 2)	1.619(2)	1.621(2)	1.620(2)	1.617(2)	1.616(2)	1.618(2)
Si2-O9	1.630(3)	1.631(2)	1.629(2)	1.628(3)	1.628(2)	1.625(2)
⟨Si2-O⟩	1.617	1.619	1.618	1.616	1.615	1.615
λ	1.0006	1.0005	1.0005	1.0005	1.0005	1.0005
σ^2	2.43	2.20	2.10	1.90	2.00	1.90
Si3-O2 (× 2)	1.626(2)	1.625(2)	1.627(2)	1.629(2)	1.628(2)	1.629(2)
Si3-O6	1.641(3)	1.641(3)	1.642(3)	1.641(3)	1.634(3)	1.638(3)
Si3-O5	1.661(2)	1.662(2)	1.663(2)	1.666(2)	1.663(2)	1.663(2)
⟨Si3-O⟩	1.639	1.638	1.640	1.641	1.638	1.640
λ	1.0050	1.0049	1.0047	1.0041	1.0039	1.0036
σ^2	20.03	19.31	18.60	16.25	15.60	14.20
O10-O4	2.960(4)	2.959(3)	2.974(3)	3.009(4)	3.039(3)	3.053(3)

Note: distances are reported in ångströms; no. *e* = mean number of electrons derived from site occupancy refinement; the mean quadratic elongation (λ) and the angle variance (σ^2) were computed according to Robinson et al. (1971).

tainty on this point expressed by Dollase (1973). Cation migration is induced by the heat treatment, as inferred from the variation in the mean electron numbers of the octahedral sites. It is noteworthy that cation disorder also affects the small and regular M2 octahedron, which, before heating, is only occupied by Al. The entry of Fe or Mn + Fe in M2 is suggested by the variation shown by the ⟨M2-O⟩ distances, which increase together with the number of electrons in M2. This is probably made possible by the loss of H during the heat treatment; indeed, when H is present, M2 accommodates Fe or Mn with difficulty because of the very short M2-H distance (2.47 Å: Kvick, 1988). An observation can be made regarding the location of Mg in the structure: for both allanite and REE-bearing piemontite, the ⟨M1-O⟩ distance, which at room temperature is greater than that observed in epidote and piemontite, has values after oxidation that are close to those predicted for a population of octahedral trivalent cations. On the contrary, with heating, the ⟨M3-O⟩ values approach but do not reach the regression lines (Fig. 2) obtained for samples containing only (Al + Fe^{3+}) and (Al + Mn^{3+} + Fe^{3+}), respectively. This is possibly be-

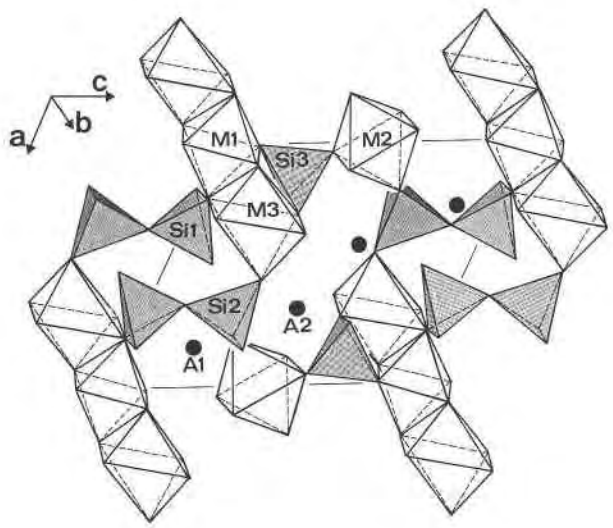

Fig. 1. Structural diagram of allanite; site labels after Dollase (1971). Only the cations of the asymmetric unit are labeled.

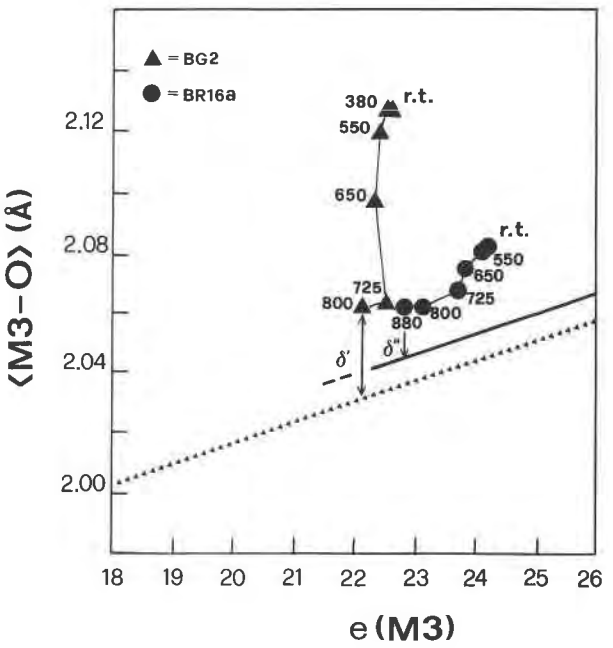

Fig. 2. The mean ⟨M3-O⟩ distance plotted against the mean electron number in the M3 site. Dotted line represents the regression line derived from clinozoisite and epidote samples (Bonazzi and Menchetti, in preparation). Solid line is derived from piemontite samples (Bonazzi and Menchetti, unpublished data).

cause of the presence of Mg in M3; however, for BR16a, it is not easy to establish whether Mg occupied M3 before the heating or if it just migrated from M1 to M3 during the heating. For this crystal, the number of electrons at M3 evolved from 24.2 (RT) to 22.8 (880 °C), thus indicating that exchange of a lighter cation for (Mn,Fe) has occurred. Because the available Mg is not enough to account for this decrease in the electron number, it can be hypothesized that minor amounts of Al also migrated from M2 to M3 upon heating. It can be noted that the shifts (δ' and δ'' in Fig. 2) of the ⟨M3-O⟩ values from the regression lines are different in the two oxidized crystals: in particular, δ'(BG2) > δ''(BR16a). This is most likely because of the different Mg content in the two crystals (0.18 and 0.06 apfu in sample BG2 and in sample BR16a, respectively).

With regard to the unit-cell parameters, the contraction related to Fe^{2+},$Mn^{2+} \rightarrow Fe^{3+}$,$Mn^{3+}$ oxidation results in a decrease of the $a \cdot b \cdot \sin \beta$ value for both crystals (Fig. 3). As already pointed out (Carbonin and Molin, 1980; Bonazzi and Menchetti, 1994), in epidote and allanite the b lattice parameter (which is parallel to the octahedral chains) is closely correlated with the ionic radius of cations entering the octahedral sites. Therefore, in sample BG2 the oxidation of Fe^{2+} to Fe^{3+} produces a marked decrease of b. The shortening along the **a** axis is much more moderate. The case of sample BR16a differs; as the heating causes an increase of the amount of Mn^{3+} (Jahn-Teller active d^4 cation), the apical M3-O4 and M3-O8 bond distances decrease more than the equatorial ones, and since the apical distances are mainly directed along the **a** axis, the a lattice parameter decreases more than b. The decrease of the volume of the M3 octahedron with the heating temperature in sample BR16a (Fig. 4) is accompanied by an anisotropic shortening of the axes; the O4-O8 octahedral axis decreases more quickly than the other two (O1-O2 × 2).

Effects of dehydrogenation

The loss of H compensating the oxidation of Fe^{2+} and Mn^{2+} is made evident by a dramatic lengthening of the

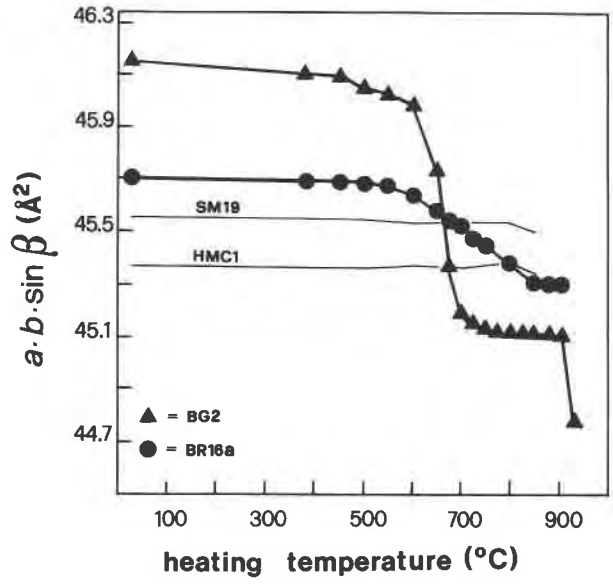

Fig. 3. The $a \cdot b \cdot \sin \beta$ value plotted against the heating temperature.

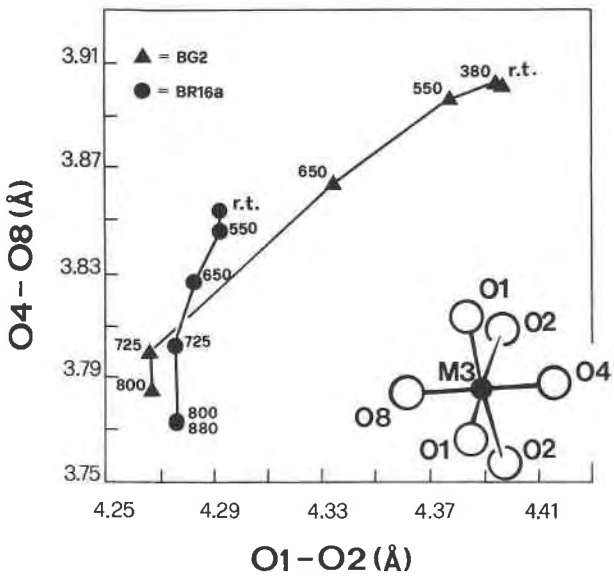

Fig. 4. The O4-O8 distance as a function of the O1-O2 distance. Both are axial interdistances of the M3 octahedron.

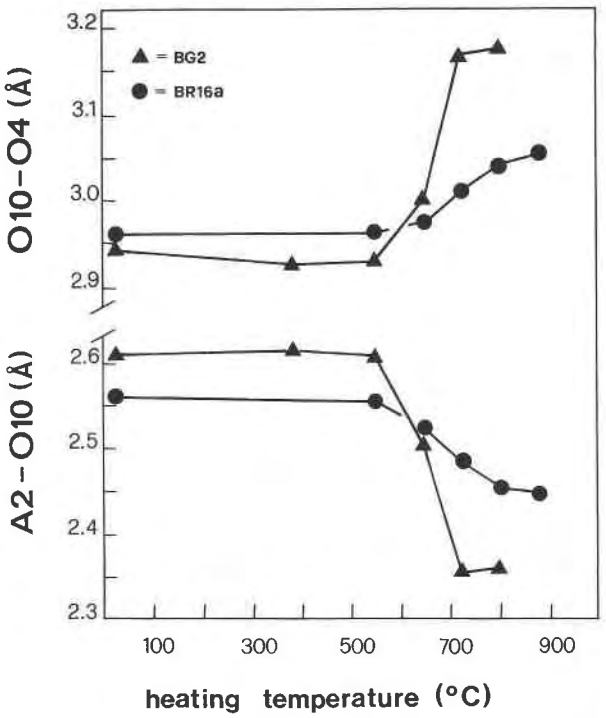

Fig. 5. The donor-acceptor distance (O10-O4) and the A2-O10 bond distance plotted against the heating temperature.

donor-acceptor (O10-O4) distance (Fig. 5). Most lengthening occurs between 600 and 725 °C in allanite and more gradually between 600 and 800 °C in the REE-bearing piemontite. In both crystals, the A2-O10 distance (Fig. 5) decreases markedly to satisfy the bond-valence requirements of O10. A lesser, but significant compensational shortening also affects the M2-O10 distance. When we compared the valence sums for O10 (Table 6) before and after the heat treatments, an increase of 0.45 vu was found for BG2. This value is very close to what we expected on the basis of the amount of available oxidizable cations, tentatively assumed to equal REE^{3+} minus Mg (apfu). If we assume for such a long O-O separation (Tables 4 and 5) that the H contributes about 0.85 vu to the valence sum of the donor (Brown and Altermatt, 1985), the total amount of H can be estimated as 0.45/0.85 = 0.53 apfu, a value very close to the number of oxidizable cations. For BR16a, a smaller variation in the bond valence sum on O10 (0.19 vu) was observed because of the lower content of REE^{3+}.

Table 6. Empirical bond-valence sums for O10

	BG2 (R7)	BG2 (800 °C)	BR16a (R7)	BR16a (880 °C)
M2	0.523	0.622	0.537	0.590
M2	0.523	0.622	0.537	0.590
A2	0.261	0.511	0.232	0.313
Total	1.307	1.755	1.306	1.493

Note: bond valences are weighted averages calculated assuming the following site populations: BG2 (R7): A2 = 0.72 REE + 0.26Ca + 0.02Th; M2 = 1.00Al. BG2 (800 °C): A2 = 0.72 REE + 0.26Ca + 0.02Th; M2 = 0.86Al + 0.14Fe. BR16a (R7): A2 = 0.77Ca + 0.21 REE + 0.02Sr; M2 = 1.00Al. BR16a (880 °C): A2 = 0.77Ca + 0.21 REE + 0.02Sr; M2 = 0.83Al + 0.17Fe. The empirical parameters used in the calculations are those of Brese and O'Keeffe (1991).

The relaxing of the H bond, which is directed along **c**, weakens the link between the M2 and the M1 + M3 octahedral chains, resulting in a lengthening of *c*. Figure 6 shows the variation of *c* as a function of the heating temperature.

Concluding remarks

The effective number of O atoms of samples HMC1 and SM19, computed for charge balance (12.505 and 12.468, respectively, Table 1), support the contention that these samples contain little to no divalent oxidizable cations. This is consistent with the observation that the values of the unit-cell parameters of HMC1 and SM19, determined at increasing temperatures, do not show appreciable variations. This observation is also in agreement with the results obtained by Catti et al. (1988) on a crystal of Sr-bearing piemontite from the type locality. They state, "No deprotonation can be obtained before the breakdown of the structure (800 °C)." For HMC1 and SM19, the structure collapsed between 850 and 900 °C.

The trends displayed by the unit-cell dimensions and selected interatomic distances show that, for allanite, the oxidation of Fe (and the corresponding H loss) starts just below 600 °C and is essentially completed at about 700–725 °C. From Mössbauer spectroscopic data on allanite from Paicoma Canyon (Dollase, 1973), it emerged that at 700 °C all Fe is present in the trivalent state; analogously, in allanite from the Rhodope Massif, only 0.80 (wt% FeO) was still present after annealing at 725 °C.

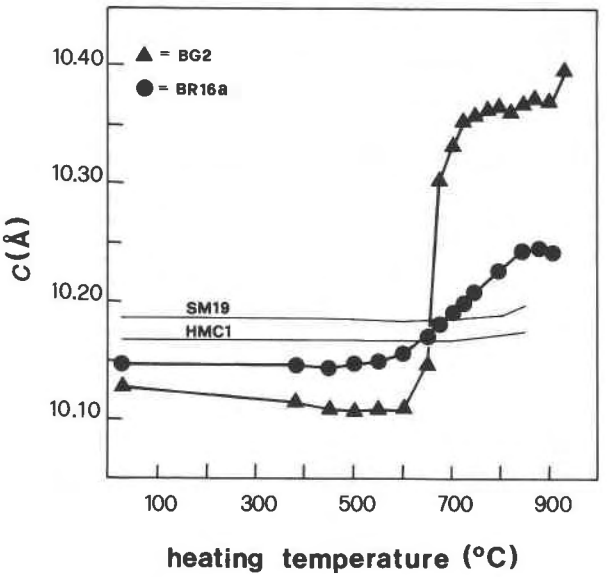

Fig. 6. The c lattice parameter plotted against the heating temperature.

Thus, it can be concluded that the variations observed for the crystal structure of BG2 before the heat treatment at 725 °C correspond with the almost complete oxidation of all the potentially oxidizable cations. According to the hypothesis that at 725 °C almost all Fe is oxidized, the unit-cell parameters (Table 2, Figs. 3 and 6) do not change significantly between 725 and 905 °C. Above this temperature, a new, marked decrease of both $a \cdot \sin \beta$ and b occurs. This is probably caused by the oxidation of Ce^{3+} to Ce^{4+}, which occurs as the structure begins to break down (between 905 and 930 °C). A few authors (Adams and Sharp, 1970; Vance and Routcliffe, 1976) have observed the precipitation of CeO_2 when the structure of allanite collapses; the present experiments suggest that oxidation of Ce^{3+} to Ce^{4+} can take place prior to the loss of structural integrity. The further increase of c that is observed between 905 and 930 °C testifies to the simultaneous loss of H, which charge balances the oxidation.

It is well known (Mitchell, 1973; Janeczek and Eby, 1993) that mineral structures expand in response to metamictization, whereas restoring crystallinity results in a decrease of the unit-cell volume. It should be noted that sample BG2 showed a moderate volume reduction during the first steps of its thermal treatment. This could suggest that slight radiation damage has affected the natural sample BG (containing 0.91 wt% ThO_2). On the other hand, the observation that the high quality of the diffraction effects in the untreated crystal did not show further improvement after heat treatment does not corroborate this interpretation.

In the case of BR16a, the oxidation-dehydrogenation process appeared to develop more gradually with the heating temperature; unlike allanite, the geometrical and structural parameters change until the heating temperature approaches about 850 °C, because of the greater difficulty with which Mn oxidizes. After the heat treatment at 930 °C, the structure of piemontite collapsed.

The correlation between the value of the β angle and the REE content observed in untreated samples (Bonazzi and Menchetti, 1994) is also worthy of attention: this relationship holds only before the oxidation-dehydrogenation process has taken place. Indeed, β increases with the heating temperature (see Table 2), thus showing values much higher than those predicted on the basis of the REE content only. This, therefore, could be a useful criterion to estimate the possible presence of the oxyallanite component in allanite.

Acknowledgments

We wish to express our gratitude to C. Gabarino, Università di Cagliari, Italy, for his help in the microprobe analysis, to P. Lattanzi, Università di Firenze, Italy, who kindly supplied us with the sample HMC1, and to O. Vaselli, Università di Firenze, Italy, who performed wet-chemical analyses. Thanks are also due to Bernd Wruck, University of Cambridge, U.K., who checked the original manuscript for its readability. Constructive reviews by T.S. Ercit and R.K. Eby are greatly appreciated. This study was funded by the C.N.R. and by M.U.R.S.T. (grant 40%).

References cited

Adams, J.W., and Sharp, W.N. (1970) A convenient nonoxidizing heating method for metamict minerals. American Mineralogist, 55, 1440–1442.

Bonazzi, P., and Menchetti, S. (1994) Monoclinic members of the epidote group: Effects of the Al = Fe^{3+} = Fe^{2+} substitution and of the entry of REE^{3+}. Mineralogy and Petrology, 51, in press.

Bonazzi, P., Garbarino, C., and Menchetti, S. (1992) Crystal chemistry of piemontites: REE-bearing piemontite from Monte Brugiana, Alpi Apuane, Italy. European Journal of Mineralogy, 4, 23–33.

Bonazzi, P., Menchetti, S., and Reinecke, T. (1993) Occurrence of REE-minerals of the epidote group in metamorphic Mn-rich rocks from Andros Island, Greece, and Varenche, Valle d'Aosta, Italy. Plinius, 10, 78–79.

Brese, N.E., and O'Keeffe, M. (1991) Bond-valence parameters for solids. Acta Crystallographica, B47, 192–197.

Brown, I.D., and Altermatt, D. (1985) Bond-valence parameters obtained from a systematic analysis of the inorganic crystal structure database. Acta Crystallographica, B41, 244–247.

Carbonin, S., and Molin, G. (1980) Crystal-chemical considerations on eight metamorphic epidotes. Neues Jahrbuch für Mineralogie Monatshefte, 205–215.

Catti, M., Ferraris, G., and Ivaldi, G. (1988) Thermal behavior of the crystal structure of strontian piemontite. American Mineralogist, 73, 1370–1376.

Dollase, W.A. (1971) Refinement of the crystal structures of epidote, allanite and hancockite. American Mineralogist, 56, 447–464.

——— (1973) Mössbauer spectra and iron distribution in the epidote-group minerals. Zeitschrift für Kristallographie, 138, 41–63.

Grew, E.S., Essene, E.J., Peacor, D.R., Su, Shu-Chun, and Asami, M. (1991) Dissakisite-(Ce), a new member of the epidote group and the Mg analogue of allanite-(Ce), from Antarctica. American Mineralogist, 76, 1990–1997.

Ibers, J.A., and Hamilton, W.C., Eds. (1974) International tables for X-ray crystallography, vol. IV, 366 p. Kynoch, Dordrecht, the Netherlands.

IGAS CSMPG (1987) International symposium on petrogenesis and mineralization of granitoids. Guangz, China, 7–10 December 1987. Field excursion guide, 24 p. Institute of Geochemistry Academia Sinica, Chinese Society of Mineralogy Petrology and Geochemistry.

Janeczek, J., and Eby, R.K. (1993) Annealing of radiation damage in allanite and gadolinite. Physics and Chemistry of Minerals, 19, 343–356.

Khvostova, V.A. (1963) On the isomorphism of epidote and orthite.

Doklady Academy of Sciences U.S.S.R., Earth Sciences Section, 141, 1307–1309.

Kumskova, N.M., and Khvostova, V.A. (1964) X-ray study of the epidote-allanite group of minerals. Geochemistry International, 4, 676–686.

Kvick, K.A., Pluth, J.J., Richardson, J.W., Jr., and Smith, J.V. (1988) The ferric iron distribution and hydrogen bonding in epidote: A neutron diffraction study at 15 K. Acta Crystallographica, B44, 351–355.

Mitchell, R.S. (1973) Metamict minerals: A review. Mineralogical Record, 4, 177–223.

Mottana, A., and Griffin, W.L. (1982) The crystal chemistry of piemontite from the type locality (St Marcel, Val d'Aosta, Italy). IMA Meeting, Varna, Reports, 635–640.

North, A.C.T., Phillips, D.C., and Mathews, F.S. (1968) A semiempirical method of absorption correction. Acta Crystallographica, A24, 351–359.

Peacor, D.R., and Dunn, P.J. (1988) Dollaseite-(Ce) (magnesium orthite redefined): Structure refinement and implications for F + M^{2+} substitutions in epidote-group minerals. American Mineralogist, 73, 838–842.

Phillips, M.W., Popp, R.K., and Clowe, C.A. (1988) Structural adjustments accompanying oxidation-dehydrogenation in amphiboles. American Mineralogist, 73, 500–506.

Phillips, M.W., Draheim, J.E., Popp, R.K., Clowe, C.A., and Pinkerton, A.A. (1989) Effects of oxidation-dehydrogenation in tschermakitic hornblende. American Mineralogist, 74, 764–773.

Robinson, K., Gibbs, G.V., and Ribbe, P.H. (1971) Quadratic elongation: A quantitative measure of distortion in coordination polyhedra. Science, 172, 567–570.

Rouse, R.C., and Peacor, D.R. (1993) The crystal structure of dissakisite-(Ce), the Mg analogue of allanite-(Ce). Canadian Mineralogist, 31, 153–157.

Rumanova, I.M., and Nikolaeva, I.M. (1960) Crystal structure of orthite. Soviet Physics: Crystallography, 4, 789–795.

Shapiro, L., and Brannock, W.W. (1962) Rapid analysis of silicate, carbonate and phosphate rocks. U.S. Geological Survey Bulletin, 1144, 1–55.

Sheldrick, G.M. (1976) SHELX: Program for crystal structure determination. University of Cambridge, England.

Sokolova, E.V., Nadezhina, T.N., and Pautov, L.A. (1991) Crystal structure of a new natural silicate of manganese from the epidote group. Soviet Physics Crystallography, 36 (2), 172–174.

Ueda, T. (1955) The crystal structure of allanite $OH(Ca,Ce)_2(Fe^{3+},Fe^{2+})Al_2OSi_2O_7SiO_4$. Memoirs of the College of Science, University of Kyoto, Series B 22, 145–163 (not seen; extracted from Mineralogical Abstracts, 14, 352, 1960).

Ungaretti, L. (1980) Recent developments in X-ray single crystal diffractometry applied to the crystal-chemical study of amphiboles. Godisnjak Jugoslavenskog Centra za Kristalografiju, 15, 29–65.

Vance, E.R., and Routcliffe, P. (1976) Heat treatment of some metamict allanites. Mineralogical Magazine, 40, 521–523.

Manuscript received February 1, 1994
Manuscript accepted June 21, 1994